Biosensors and Bioelectronics 55 (2014) 452–458

Contents lists available at ScienceDirect

Biosensors and Bioelectronics

journal homepage: www.elsevier.com/locate/bios

# *In-situ* detection of density alteration in non-physiological cells with polarimetric tilted fiber grating sensors

Tuan Guo [a], Fu Liu [a], Yu Liu [b], Nan-Kuang Chen [c], Bai-Ou Guan [a,*], Jacques Albert [d,**]

[a] Institute of Photonics Technology, Jinan University, Guangzhou 510632, China
[b] Department of Biochemistry, Medical School, Jinan University, Guangzhou 510632, China
[c] Department of Electro-Optical Engineering, National United University, Miaoli 360, Taiwan
[d] Department of Electronics, Carleton University, 1125 Colonel By Drive, Ottawa, Canada, K1S 5B6

ARTICLE INFO

*Article history:*
Received 9 October 2013
Received in revised form
22 December 2013
Accepted 23 December 2013
Available online 1 January 2014

*Keywords:*
Polarimetric fiber grating
Optical fiber
Optical biosensor
Density alteration in non-physiological cells

ABSTRACT

Tilted fiber Bragg grating (TFBG) biosensors can be used as a cost-effective and relatively simple-to-implement alternative to well established biosensor platforms for high sensitivity biological sample measurements in situ or possibly in vivo. The fiber biosensor presented in this study utilizes an in-fiber 12° tilted Bragg grating to excite a strong evanescent field on the surface of the sensor over a large range of external medium refractive indices. The devices have minimal cross-sensitivity to temperature and their fabrication does not impact the structural integrity of the fiber and its surface functionalization. Human acute leukemia cells with different intracellular densities and refractive index (RI) ranging from 1.3342 to 1.3344 were clearly discriminated *in-situ* by using the differential transmission spectrum between two orthogonal polarizations for the last guided mode resonance before "cut-off", with an amplitude variation sensitivity of $1.8 \times 10^4$ dB/RIU, a wavelength shift sensitivity of 180 nm/RIU, and a limit of detection of $2 \times 10^{-5}$ RIU. The detection process was precisely controlled with a micro-fluidic chip which allows the measurement of nL-volumes of bio-samples. The proposed in-fiber polarimetric biosensor is an appealing solution for rapid, sub-microliter dose and highly sensitive detection of analytes at low concentrations in medicine, chemical and environmental monitoring. @ 2013 Elsevier B.V. All rights reserved.



## 1. Introduction

The detection of small changes in biological samples, due to cell growth or death for instance, is often carried out in aqueous solutions (saline). Such changes are inevitably associated with refractive index (RI) changes, and some of the most sensitive bio-detection methods (like surface plasmon resonance (SPR) sensors and resonant waveguide grating sensors) are actually based on very sensitive refractometry. It was recently demonstrated that drug response and pathological changes in cells which were separated from a human acute leukemia cell line (K562) by using discontinuous sucrose gradient centrifugation (DSGC) were associated with intracellular density changes (Liu et al., 2011). It is the purpose of this paper to demonstrate that a simple tilted fiber Bragg grating refractometer (TFBG) can be used to monitor those intracellular density changes effectively, thanks to a novel data analysis method for the differential polarimetric spectral transmission of the TFBG. In particular, the discrimination of a group of biological samples, named S40, S50 and S60, has been achieved through a high sensitivity RI measurement by using a 12° TFBG sensing probe. By comparing the slight RI difference between S40, S50 and S60 (ranging from 1.3342 to 1.3344), we studied the relationship between the intracellular density of cells and their RI, which might provide a potential way to verify the hypothesis for "density alteration in non-physiological cells (DANCE)" in response to drugs and pathological changes in cells (Liu et al., 2011). However, the mechanisms of DANCE are not clear. It has been hypothesized that change of metabolism mode, change of cell membrane function, and pathological changes in the cells might be the causes for DANCE. Therefore, study of DANCE might be helpful to the understanding of drug resistance, development of new drugs, separation of new subtypes from a cell population, forensic analysis, and discovery of new physiological or pathological properties of cells.

## 2. Polarimetric TFBG sensor

Fiber sensors are ideally suited for rapid, μL-volume and sensitive detection of analytes at low concentrations in medicine, environmental monitoring and food safety, because the sensing platform is compact (cm in-length, compatible with optofluidic

* Corresponding author. Tel.: +82 20 85220065; fax: +86 20 85222046.
** Corresponding author. Tel.: +1 613 5202600x5578; fax: +1 613 5205708.
*E-mail addresses:* tguanbo@jnu.edu.cn (B.-O. Guan), jacques_albert@carleton.ca (J. Albert).

0956-5663/$ - see front matter © 2014 Elsevier B.V. All rights reserved.
http://dx.doi.org/10.1016/j.bios.2013.12.054

microsystems) and cost-effective (well-established grating fabrication process, existing broad base of commercial instrumentation for sensor interrogation, such as LEDs, laser diodes, photodiodes, and CCDs). Fiber optic also allows for data collection in situ and remotely from large distances (Leunga et al., 2007; Fan et al., 2008; Homola, 2008). Of the many possible fiber optic biochemical sensing schemes, the recently developed TFBG platform is generating interest because of its many unique properties (Albert et al., 2013). High resolution sensing is achieved by measuring the positions of resonances in the transmission (or reflection) spectrum that have: (1) high sensitivity, up to 500–1000 nm of wavelength shift per unit change in refractive index; (2) narrow linewidths (100 pm and less); (3) high signal-to-noise ratio ( $>40$ dB) because of the use of low loss fibers and devices; (4) temperature insensitivity arising from the absolute power and wavelength reference provided by the resonance of the core mode guided light. These features have led to demonstrated limits of detection of $10^{-5}$ in refractive index (Caucheteur et al., 2011) and $10^{-12}$ M in protein concentrations in solution (Lepinay et al., 2014). Finally, TFBGs are easy to manufacture and do not require physical deformation or degradation of the fiber itself, thereby ensuring device reliability and low fabrication cost in volume quantities (TFBG use the same manufacturing platform as the un-tilted FBGs that are widely deployed in the telecommunications and structural sensing industries).

The sensing principle of the TFBG refractometer proceeds as follows. Incoming core guided light interacts with a permanent refractive index grating that has been inscribed in the fiber by intense ultraviolet light irradiation through a diffractive phase mask. A tilt in the orientation of the grating planes favors the coupling of light to modes guided by the cladding instead of the core (Fig. 1a). Since the cladding diameter is very large ( $>100$ μm, almost 100 times the wavelength) a large number of modes can be excited, each at a specific wavelength, resulting in a fine comb of resonances in the transmission spectrum of the grating (Caucheteur et al., 2013). The resonance with the longest wavelength corresponds to the most well guided mode, the single core guided mode in the fibers that are used for this work. This resonance is inherently insensitive to events outside the cladding and is used as a power and wavelength reference (all the core and cladding mode resonances have the same temperature dependence and hence shift together with temperature, thereby removing the influence of this parameter on measurements) (Chan et al., 2007). Further resonances at decreasing wavelengths correspond to cladding guided modes with increasing amounts of evanescent fields extending outside the cladding boundary (typically over a thickness of the order of 2 μm above the cladding surface). When the immediate environment of the TFBG changes within the region sampled by the mode evanescent fields, the resonance positions of the corresponding cladding modes change accordingly (Fig. 1b). The largest resonance shift occurs when the evanescent field of the modes overlaps maximally with the perturbation, usually for the least guided resonances, i.e., at the shortest wavelengths (Chan et al., 2007). However, at further decreasing wavelengths there comes a point at which the grating couples light to modes that are no longer guided by the cladding. These leaky modes have resonance positions that do not shift in wavelength in response to outside refractive index changes, but only in amplitude (Laffont and Ferdinand, 2001; Chen et al., 2008). The boundary between guided and leaky modes is called the “cut-off point” (as the red stars marked in Fig. 1b) and the last guided mode before this point has the maximum extent of evanescent field penetration in the external medium (and hence the largest sensitivity). The operating point (i.e., the range of wavelengths where modes have maximum sensitivity, near the “cut-off point” for instance) determines the choice of tilt angle: increasing the tilt angle shifts the maximum of the resonance amplitudes towards lower wavelengths (Albert et al., 2013). Finally, a further mode selection mechanism can be used to refine the sensing capabilities of the TFBG. By launching linearly polarized light in the core, two very different families of cladding modes can be selected: modes with radially polarized evanescent fields (hereafter named P-modes, as they are P-polarized relative to the tilt plane), and modes with azimuthally polarized evanescent fields (S-modes) (Caucheteur et al., 2011; Thomas et al., 2012; Alam and Albert, 2013; Guo et al., 2013). Fig. 1c shows the horizontal component of the electric field for representative S- and P-modes. Since S- and P-modes have different reflection characteristics at the boundary, a comparison of the relative changes observed in a pair of S- and P-modes provides a self-referenced tool to measure even smaller changes at the cladding surface than un-polarized TFBGs (Voisin et al., 2011; Caucheteur et al., 2013; Voisin et al., 2014). In this paper, we present new analysis techniques that make optimum use of this difference. These techniques are introduced in Section 4.

For bio-chemical applications, the TFBG can be used for label-free sensing when provided with a functionalized coating whose refractive index can be modified by the selective attachment of certain types of molecules or cells. The same label free techniques

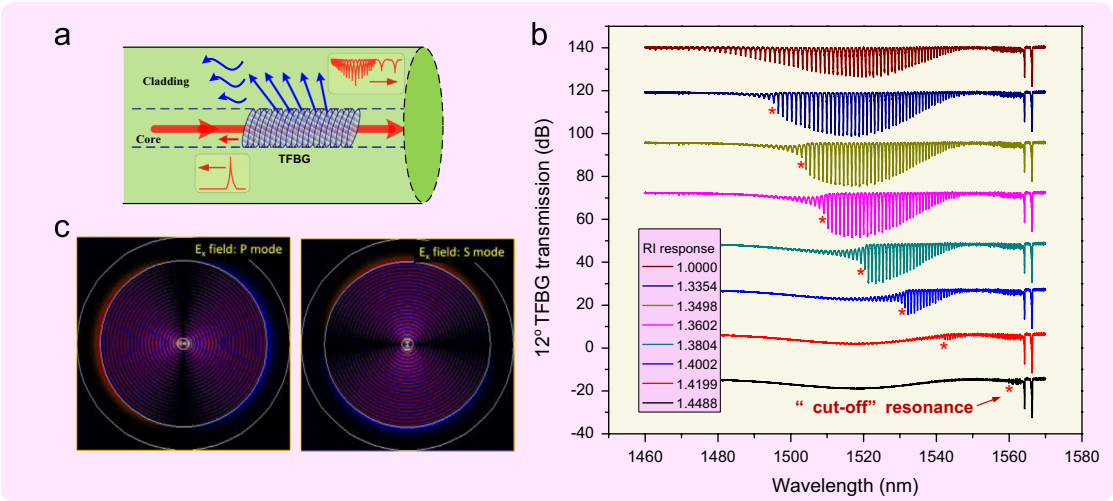


**Fig. 1.** Polarimetric TFBG sensor: (a) schematic diagram of TFBG, (b) spectral response of 12° TFBG versus surrounding RI, (c) simulated horizontal component of the transverse electric field of representative S- and P-modes near “cut-off”.

that have been demonstrated for interferometric sensors such as whispering gallery mode devices (Vollmer and Arnold, 2008; Wang et al., 2012; Arnold et al., 2012; Dantham et al., 2012) and ring cavity sensors (Candiani et al., 2012), surface plasmon resonances devices (Homola, 2008; Pollet et al., 2009; François et al., 2011) as well as grating based devices in microstructured (Boehm et al., 2011; Candiani et al., 2013) or etched fibers (Zhang et al., 2005; Chen et al., 2010; Chen et al., 2013) can, and have been applied to TFBGs (Maguis et al., 2008; Shevchenko et al., 2011; Voisin et al., 2014). While the TFBG provides a more robust sensing property than most of the other label free methods (for the reasons listed above), it cannot compete with resonator types in the detection of very small amounts of material, down to the single molecule limit. This is because the high finesse of the resonances comes from coupling over "large" distances of the order of mm to cm, and their response to biochemical changes represents an average over the whole grating length.

In this paper, new results are presented for the optimization of a new TFBG sensing modality based on polarimetric differential measurement of the last guided mode resonance above cut-off for the measurement of intracellular density changes that are revealed by small changes in the refractive index of the medium containing the cells. The required solution volume for full sensor resolution consists of a 2 μm thick ring around the 125 μm diameter cladding, over a length of 1 cm, i.e., a volume of only 4 nL.

## 3. Materials and methods

### 3.1. Fabrication of TFBG biosensor

The sensor was manufactured using the techniques reviewed in (Albert et al., 2013), i.e., in a commercial single-mode fiber (photosensitive fiber) with a TFBG inscribed in the fiber core. The TFBG was manufactured using the phase-mask technique: it required shining of UV light at 193 nm onto the surface of a bare fiber through the mask with the required grating pattern. The grating planes were written with a certain tilt relatively to the longitudinal axis of the fiber (Fig. 1a). The tilt of the grating is an important parameter that can be used to choose which set of cladding modes is going to be excited. As a result, it makes it possible to adjust the operating range of the sensor in order to optimize the response for certain refractive indices. Here, the gratings had a tilt of 12°, which maximizes the amplitude of the resonances in aqueous solutions with refractive indices around 1.32–1.34. As shown in Fig. 1b the grating resonances remain well defined up to indices of 1.4, but it would be obviously preferable to decrease the tilt angle (to 6° for instance, as indicated in (Albert et al., 2013)) in order to maximize the depth of the last guided resonance at these values of external refractive index and thus increase the signal to noise ratio.

### 3.2. Bio-samples preparation (human acute leukemia cells)

Previous study shows that reverse transcription-polymerase chain reaction (RT-PCR) results varied in a significantly great range. The poor repeatability of the RT-PCR results could not be explained by the standard deviation of the method. Even under same experimental conditions cells responded quite differently to a same drug.

To find out if there were different cells in a cell line with different sensitivities to a drug, we tried to separate human acute leukemia cells (K562) by using discontinuous sucrose gradient centrifugation (DSGC). As expected, the cells under normal culture conditions (with the concentrations of $2 \times 10^5$/ml) were separated into two bands, which stop at the top of the layer of 50% and the layer of 60% (w/v) sucrose (Fig. 2c, A1), and the cells in "bad conditions" (after more than 20 passages) showed two more bands at 30% and 40% sucrose layers (Fig. 2c, A2). The result indicated that a cell line under same conditions existed in different physiological or pathological statuses with different intracellular densities. From these experiments we found that in a cell population the difference in intracellular density of cells was associated with different drug responses and with different expression levels of some genes.

For convenience, the intracellular density change due to drugs or environmental changes was named as "Density Alteration in Non-physiological Cells", or DANCE. "Non-physiological cells" were the cells under non-physiological or non-naturally living conditions, or those that were undergoing pathological changes. A band in DSGC was labeled as "S" with the number of sucrose concentration at which the cells stop. For example, if a band of cells stop at the top of a layer of 50% (w/v) sucrose it was labeled as "S50", and so on. As band S30 is not easy to culture, here in this work we use the bands S40, S50 and S60 as detected analytes.

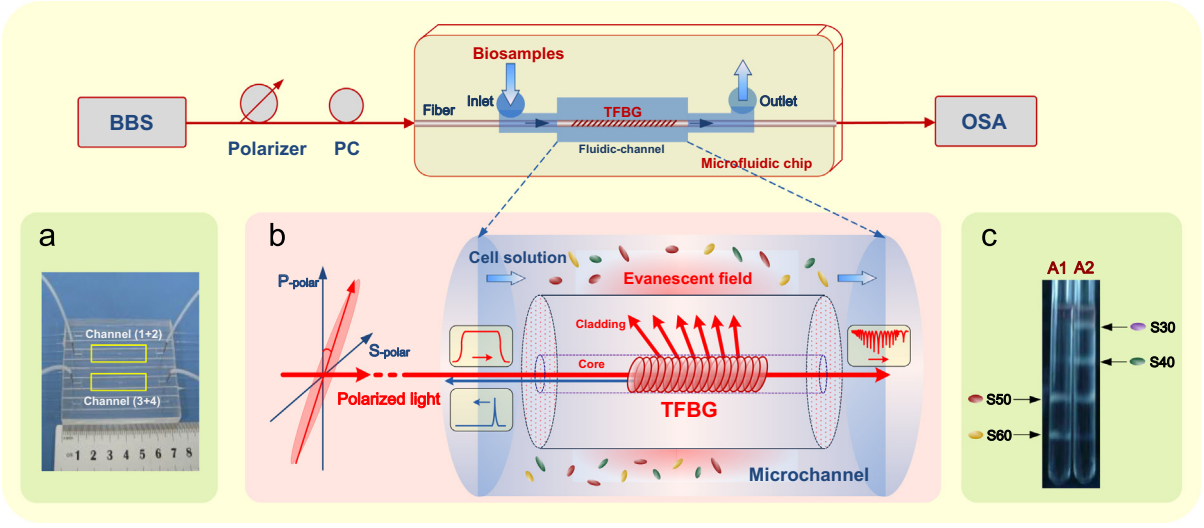


**Fig. 2.** Polarimetric TFBG sensing system: (a) micro-fluidic chip for biosamples measurement, (b) schematic diagram of polarimetric TFBG biosensor interrogated with tunable linearly polarized light, (c) bio-samples (human acute leukemia cell lines, i.e., S40, S50, S60) associated with different intracellular density which were separated by discontinuous sucrose gradient centrifugation (DSGC).

### 3.3. Experimental setup and optical configuration

The experimental setup required the sensor to operate in the transmission regime. During the experiments, the sensors were fixed in PDMS-based micro-fluidic channels designed specifically for the biosensing tests. While each individual sensor was fixed in the micro-channel (width 200 μm by height 150 μm) with help of UV-sensitive adhesive both sides over the sensing element of 2 cm in length (for a total sensing volume of 35 μL, taking into account the volume taken up by the fiber). Biosample solutions were injected into the micro-fluidic chip (Fig. 2a) via an electronic-controlled pump, eliminating the potential environmental influence during the bio-sample measurement.

The sensing TFBG was excited by a broadband source (BBS) with light over the 1480–1640 nm range and its transmission spectrum was monitored by an optical spectrum analyzer (OSA) with minimum wavelength resolution of 0.002 nm. A linear polarizer and polarization controller (PC) were placed upstream of the TFBG to adjust and orient the state of polarization of light launched into fiber grating, so as to ensure the strongest contrast between the two orthogonal polarizations (P and S polarization). The measurement resolution was set at 0.01 nm, and measurements were recorded continuously at a rate of one spectrum every 1.2 s. A schematic of the optical setup is shown in Fig. 2.

## 4. Results and discussion

### 4.1. Characterization of the polarimetric TFBG biosensors

Fig. 3 shows the spectral response of a 12° TFBG in a saline solution (RI=1.3340) versus different orientations of linearly polarized input light. The resonances clearly show a maximum and minimum transmission states as a function of polarization orientation and we label these as P and S polarization (as they correspond to light polarized in the plane and out of the plane of

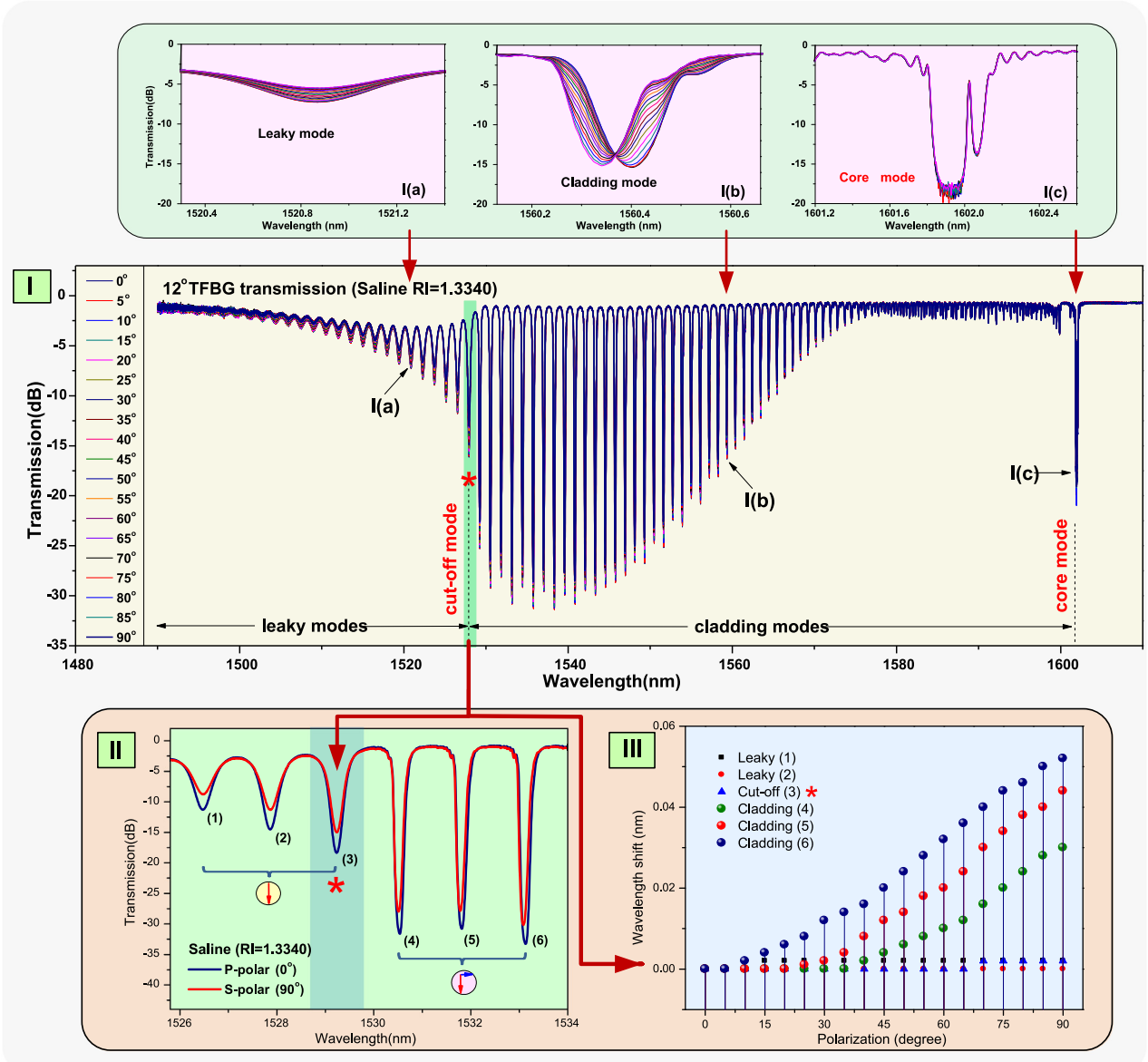


**Fig. 3.** Spectral transmission characteristics of a 12° TFBG in saline versus different orientations of the input light polarization: (I) whole spectrum (about 120 nm) and specific resonances of interest (I(a) leaky mode, I(b) cladding mode and I(c) core mode, less than 1 nm each), (II) and (III) present the orthogonal-polarimetric spectral response of TFBG around the "cut-off" region and the corresponding wavelength shifts of the resonances shown. *Note*: the "cut-off" mode is marked by red asterisk "*". (For interpretation of the references to color in this figure, the reader is referred to the web version of this article.)

tilt, respectively). As shown in part I of Fig. 3, the transmission of the TFBG can be generally divided into three groups of modes, i.e., the core mode (located at the longest wavelength and totally immune to any polarization and SRI perturbations), the cladding modes (hundreds of cladding-guided resonances with strong polarization dependence and high sensitivity to SRI), and the leaky modes (modes with effective indices larger than the surrounding RI, and therefore not totally internally reflected at the cladding boundary). The boundary between cladding and leaky modes is indicated by a sudden increase in the loss of the modes, evidenced by reduced amplitude of the cladding mode resonance (the red asterisk "*" marked in Fig. 3I). Another "signature" of the leaky mode regime is the absence of wavelength shift as a function of input polarization angle (Fig. 3Ia). This is due to the fact that the effective index of guided modes depends in part on the phase of the Fresnel reflection coefficients at the cladding-outer medium boundary. Since the phase of the Fresnel reflection coefficients only depend on polarization for totally internally reflected light (i.e., guided modes), only those modes will wavelength shift as the polarization rotates.

Finding the most sensitive resonance to surrounding RI consist of determining the last guided mode before the leaky mode regime, but the exact determination of the "cut-off" mode is not evident in the insertion loss spectra. We show below that the polarimetric information makes this determination straightforward.

### 4.2. Detection of bio-samples

Fig. 4 shows the experimental transmission spectra of 12° TFBG in the air, different cell suspensions (i.e., leukemia cells S40, S50 and S60 separated by DSGC, with the same concentration of $5 \times 10^6$/ml, and RI range between 1.3342 and 1.3344), and the buffer solution (saline RI ~1.3340) for control. For the very slight RI changes (less than 0.0002) associated with the biological solutions S40, S50 and S60, it is hard to discriminate them directly in transmission (the "cut-off" modes of all the bio-samples appear to be at the same wavelength indicated by red arrows in Fig. 4a). A clearer picture is obtained from the difference between the S and P spectra in the spectral region near the "cut-off" mode, shown in Fig. 4b. These "polarimetric-differential spectra" allow for the visualization of smaller shifts because of the high spectral slopes of the resonances considered. Any small wavelength shift will result in both a positive and a negative peak in the differential spectrum, while amplitude only changes will be unipolar (negative in the case of increasing RI). The "last guided" mode is clearly identified in the inset of Fig. 4b as the shortest wavelength mode with a bi-polar differential spectrum, and it will provide the most sensitive measure of the difference between the cell lines because this mode has the highest penetration in the cell solution.

Fig. 4c shows a zoomed-in differential spectrum with positive wavelength shifts and negative amplitude changes, which indicate

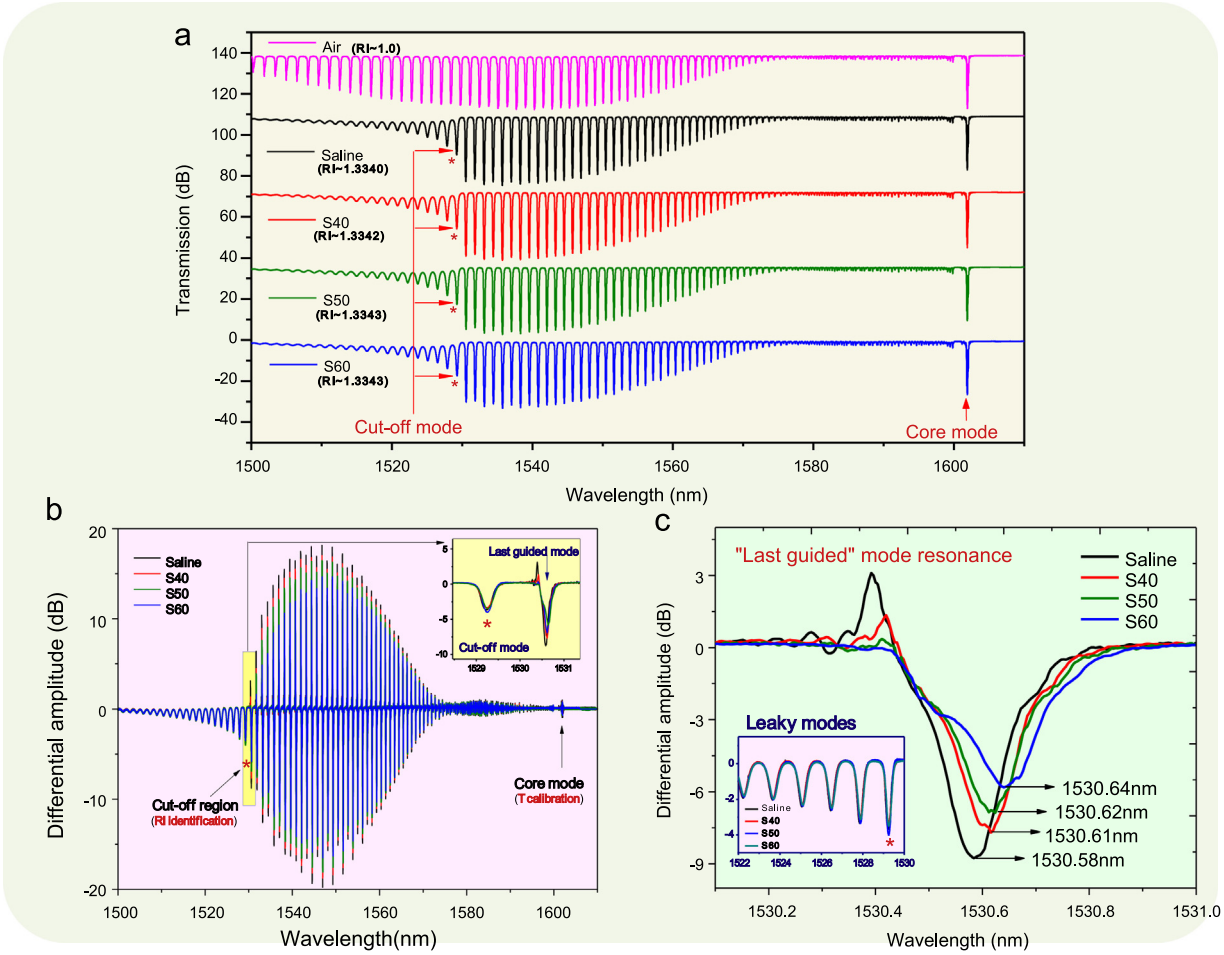


**Fig. 4.** Experimental results and analysis of biosamples measurement: (a) spectral response of 12° TFBG in air, saline and different cell sample solutions. The arrows (and asterisks) point to the "cut-off" and core mode resonances for each sample solution, (b) differential transmission spectra of P- and S-polarizations of 12° TFBG versus cell sample solutions. The inset zooms in the spectrum near the "cut-off" resonance. The core mode (the longest wavelength resonance) is used to cancel temperature-induced spectral shifts, (c) zoomed-in differential transmission of P- and S-polarizations near the "cut-off" mode versus cell samples. The inset shows the actual P-polarized spectra on the short wavelength side of the "cut-off" mode resonance.

positive RI changes, in going from the S40 to S50 and S60 cell types. This agrees with the fact that S60 contains mostly "younger" leukemia cells with higher intracellular densities, while the S40 contains mostly "older" ones (Liu et al., 2011). When the refractive indices of the cell and saline solutions are considered, exposition of the TFBG to the various DSGC separated cells in saline solutions results in a wavelength and amplitude shifts of the negative differential peak of that are superior to those obtained with TFBG refractometers without polarimetric control (Chan et al., 2007), and approach that of plasmon-assisted TFBG polarimeters (Caucheteur et al., 2013), without the need for a precise gold metal film coating on the fiber.

As will be demonstrated below, this large sensitivity is obtained with high accuracy thanks to Q-factor of these resonances (the Q-factor being defined as the wavelength divided by the spectral width at half maximum), which is larger than $10^5$ (for our spectral widths between 0.01 and 0.1 nm), as well as to the inherent low loss of the fibers which results in a high signal to noise ratio (greater than 30 dB).

### 4.3. Real-time response and data processing

The proposed TFBG sensor shows a quick response (1.2 s per full scan) and clearly identified spectral signature for *in-situ* measurements of different bio-samples (S40, S50 and S60, corresponding to cells with different intracellular densities, separated by saline solution injections between each bio-sample change). Detailed experimental results and data analysis are shown in Fig. 5. By zooming in on the differential transmission spectra (orthogonal P- and S-polarizations) of the last guided mode for (Fig. 5a), the polarimetric TFBG sensor provides two ways to extract sensing information. One is wavelength domain (by monitoring the dip wavelength shift as shown in Fig. 5b), which provides a real time response versus cell sample solutions, with a wavelength shift sensitivity of 180 nm/RIU. The noise during each of the constant RI phases is of the order of $\pm 2$ pm. The sensor response clearly returns to the same level upon re-injection of the saline solution (within the aforementioned noise limits). Another way to read the sensor is in the amplitude domain (provided by the peak-to-peak differential amplitude of the last guided mode as shown in Fig. 5c). The amplitude sensitivity reaches $1.8 \times 10^4$ dB/RIU, which separates the S40 from the S50 and S60 resonances by 2 and 3 dB respectively. The amplitude approach has a stability (or reproducibility) of $\pm 0.14$ dB over repeated measurements. It is interesting to note that both the wavelength and amplitude sensitivities and corresponding statistical errors yield a similar limit of detection of $2 \times 10^{-5}$ in refractive index. Such limit of detection is comparable to the best results obtained with more complex SPR-based fiber sensors (Homola, 2008; Shevchenko et al., 2011; Caucheteur et al., 2013; Voisin et al., 2014), but without the need to coat the fiber with a precise nanometer scale metal coating. Temperature self-calibration where spectral shifts due to temperature changes can be eliminated by referencing all wavelengths to the core mode (Fig. 4b), which is unaffected by the surrounding RI and has the same temperature dependence with the other modes (Chan et al., 2007), thereby ensuring that the differential spectra are due solely to surround RI changes (different biosample solutions). The fact that the amplitude measurements are differential automatically results in cancellation of any power level or temperature fluctuation effects from the measurements and ensures a maximum signal to noise ratio. This amplitude discrimination method is derived from

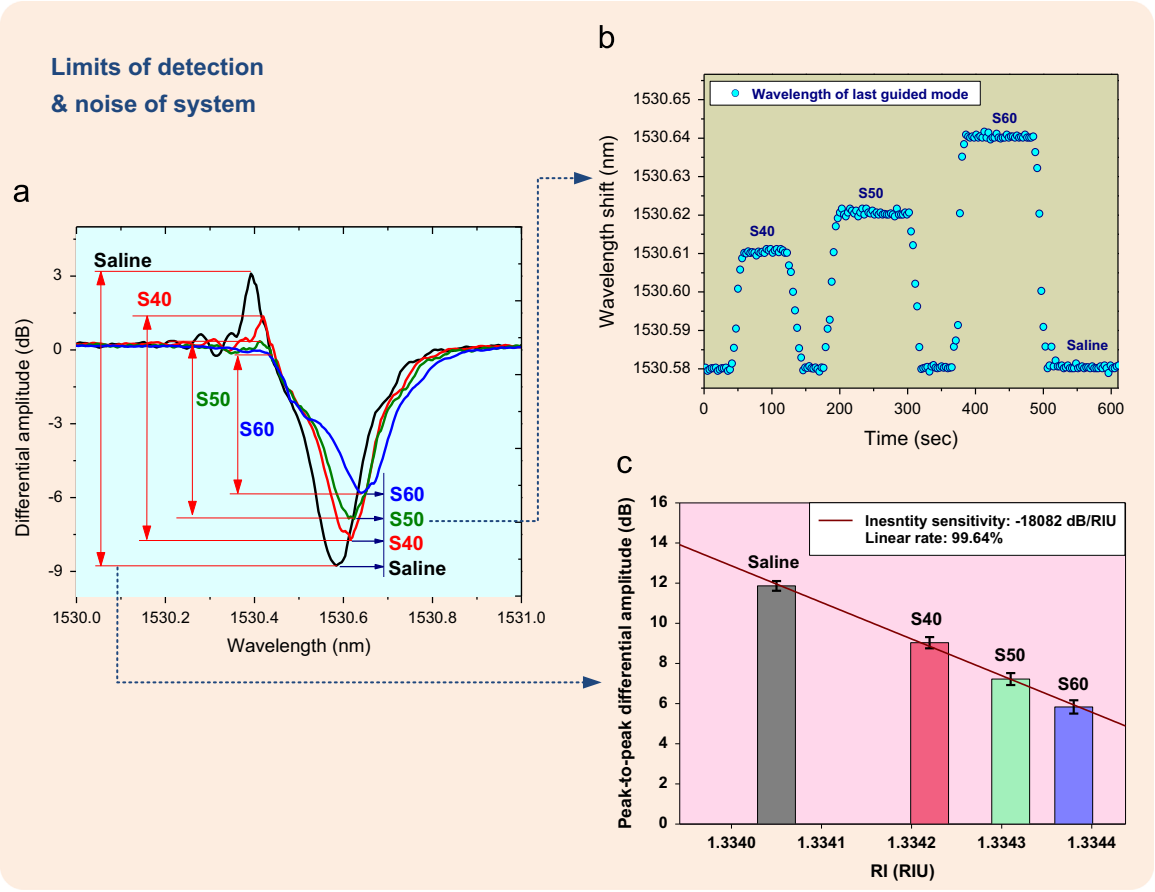


**Fig. 5.** The sensitivity, limits of detection and noise of sensing system: (a) zoomed-in spectra of the last guided mode versus cell sample solutions, (b) the real-time wavelength response and (c) peak-to-peak differential amplitude (with error bar) of the last guided mode versus cell samples (and their refractive index).

that used previously in SPR-TFBG sensors (Voisin et al., 2011; Shevchenko et al., 2011) but applied here to a bare TFBG refractometer for the first time and demonstrating very high sensitivity, because of the clearer identification of the "cut-off" mode resonance.

## 5. Conclusion

In summary, we have demonstrated measurements of intracellular cell density with a simple TFBG refractometer used in differential polarimetric mode. This mode of operation clearly identifies the most sensitive modal resonance, i.e., the resonance corresponding to the last guided cladding mode before the leaky mode regime. Furthermore the differential spectrum approach automatically cancels the effect of temperature and power level fluctuations. The minimum detectable refractive index change of $2\times10^{-5}$ is comparable to that obtained with the best SPR-assisted fiber-optic sensors, without the need for a precisely deposited nanoscale metal layer. The associated high refractometric sensitivity ($1.8\times10^{4}$ dB/RIU) allowed for the discrimination of low concentrations of Leukemia cells at various stages of their lives. Combined with micro-fluidic technology, the detection process can be precisely controlled with as little as μL-volumes of biosamples. The sensor itself is very easy to manufacture at very low cost and to interrogate using standard telecommunications-based instrumentation. Therefore, it is a good candidate for rapid and highly sensitive detection in microliter volumes of analytes at low concentrations ($\sim10^{5}$ cells/ml) in medicine, chemical and environmental monitoring.

## Acknowledgment

This work was funded by the National Natural Science Foundation of China (No. 61205080), National Innovation Fund for Technology (No. 2C26214405312), Guangdong Natural Science Foundation of China (No. S2012010008385), Doctoral Program of Higher Education of China (No. 20114401120006, No. 20114401110006), Pearl River Scholar for Young Scientist (No. 2011J2200014). J. Albert acknowledges the support of the Natural Sciences and Engineering Research Council of Canada (NSERC) and Canada Research Chair Program.

## References

Alam, M.Z., Albert, J., 2013. J. Lightwave Technol. 31 (19), 3167–3175.
Albert, J., Shao, L.Y., Caucheteur, C., 2013. Laser Photon. Rev. 7 (1), 83–108.
Arnold, S., Dantham, V.R., Barbre, C., Garetz, B.A., Fan, X.D., 2012. Opt. Express 20 (24), 26147–26159.
Boehm, J., François, A., Ebendorff-Heidepriem, H., Monro, T.M., 2011. Plasmonics 6 (1), 133–136.
Candiani, A., Bertucci, A., Giannetti, S., Konstantaki, M., Manicardi, A., Pissadakis, S., Cucinotta, A., Corradini, R., Selleri, S., 2013. J. Biomed. Opt. 18 (5), 057004-1–057004-6.
Candiani, A., Sozzi, M., Cucinotta, A., Selleri, S., Veneziano, R., Corradini, R., Marchelli, R., Childs, P., Pissadakis, S., 2012. IEEE J. Sel. Top. Quant. Electron. 18 (3), 1176–1183.
Caucheteur, C., Chen, C., Voisin, V., Berini, P., Albert, J., 2011. Appl. Phys. Lett. 99 (4), 041118. (3).
Caucheteur, C., Voisin, V., Albert, J., 2013. Opt. Express 21 (3), 3055–3066.
Chan, C.F., Chen, C., Jafari, A., Laronche, A., Thomson, D.J., Albert, J., 2007. Appl. Opt. 46 (7), 1142–1149.
Chen, C.H., Tsao, T.C., Tang, J.L., Wu, W.T., 2010. Sensors 10 (5), 4794–4804.
Chen, C.K., Guo, T., Laronche, A., Albert, J., 2008. Radiation mode resonances of tilted fiber Bragg gratings for high index media measurement. In: Proceedings of the SPIE 7004, International Conference on Optical Fibre Sensors, 700418, http://dx.doi.org/10.1117/12.785661.
Chen, N.K., Yang, T.H., Chen, Y.N., Guo, T., Guan, B.O., 2013. Appl. Phys. Lett. 102 (17), 171101. (3).
Dantham, V.R., Holler, S., Kolchenko, V., Wan, Z., Arnold, S., 2012. Appl. Phys. Lett. 101 (4), 043704. (4).
Fan, X., White, I.M., Shopova, S.I., Zhu, H., Suter, J.D., Sun, Y., 2008. Anal. Chim. Acta 620 (1–2), 8–26.
François, A., Boehm, J., Oh, S.Y., Kok, T., Monro, T.M., 2011. Biosens. Bioelectron. 26 (7), 3154–3159.
Guo, T., Zhang, Z.C., Liu, F., Zhu, X.Y., Liu, Y., Guan, B.O., Albert, J., 2013. IEEE Adv. Infocomm Technol. (ICAIT), 242–243.
Homola, J., 2008. Chem. Rev. 108 (2), 462–493.
Laffont, G., Ferdinand, P., 2001. Electron Lett. 37 (5), 89–290.
Lepinay, S., Staff, A., Lanoul, A., Albert, J., 2014. Biosens. Bioelectron. 52, 337–344.
Leunga, A., Shankarb, P.M., Mutharasan, R., 2007. Sens. Actuators B: Chem. 125 (2), 688–703.
Liu, Y., Wei, J.G., Wu, B., Wu, X.H., Lan, F.F., Zhu, Y.C., Wang, M., Li, H.C., Li, L.N., Li, J.X., Fei, J., 2011. Nat. Preced..
Maguis, S., Laffont, G., Ferdinand, P., Carbonnier, B., Kham, K., Mekhalif, T., Millot, M.C., 2008. Opt. Express 16 (23), 19049–19062.
Pollet, J., Delport, F., Janssen, K.P.F., Jans, K., Maes, G., Pfeiffer, H., Wevers, M., Lammertyn, J., 2009. Biosens. Bioelectron. 25 (4), 864–869.
Shevchenko, Y., Francis, T.J., Blair, D.A.D., Walsh, R., DeRosa, M.C., Albert, J., 2011. Anal. Chem. 83 (18), 7027–7034.
Thomas, J.U., Jovanovic, N., Krämer, R.G., Marshall, G.D., Withford, M.J., Ťunnermann, A., Nolte, S., Steel, M.J., 2012. Opt. Express. 20 (19), 21434–21449.
Voisin, V., Caucheteur, C., Mégret, P., Albert, J., 2011. Appl. Opt. 50 (22), 4257–4261.
Voisin, V., Pilate, J., Damman, P., Mégret, P., Caucheteur, C., 2014. Biosens. Bioelectron. 51, 249–254.
Vollmer, F., Arnold, S., 2008. Nat. Methods 5 (7), 591–596.
Wang, H.Z., Yuan, L., Kim, C.W., Han, Q., Wei, T., Lan, X.W., Xiao, H., 2012. Opt. Lett. 37 (1), 94–96.
Zhang, Y., Gu, C., Schwartzber, A.M., Zhang, J.Z., 2005. Appl. Phys. Lett. 87 (12), 123105. (3).